Independent Study

THE USE OF MICROEARTHQUAKES IN MAPPING THE BASE OF THE LOW RIGIDITY LAYER BENEATH SOCORRO, NEW MEXICO

A report presented in partial
fulfillment of the requirements
for the degree of
Master of Science in Geophysics

by

Tarek Mostafa Hassen-Bey

April, 1974

Contents

Illustrations

Illustrations (Cont.)

Abstract

SNM station seismograms immediately after S_xS phase showed a consistent reflected S-phase energy arrival. This reflected energy is believed to come from a sharp discontinuity 20.88 Km deep and dipping 5° toward the north. This deep discontinuity might be the base of a low rigidity layer beneath the Socorro area with partially molten material which is increasing in thickness north of Socorro.

Introduction

This report is a continuation of the work of Sanford, et al. (1973) in using reflected phases on microearthquake seismograms to determine the depths and the characteristics of the different velocity discontinuities beneath the Rio Grande rift near Socorro. A late reflected S-wave energy is observed after the reflected phases studied by Sanford, et al. (1973). The late reflected S-phase is believed to come from the base of the low rigidity layer which is dipping northward from Socorro.

The Rio Grande Rift

The structure of the Rio Grande rift is linked depressions with raised margins. The rift is badly shattered with normal faulting and evidence of the vertical movement continuing to the present (Sanford, et al., 1972). The rift structure near Socorro is intergraben horsts extending northward from Socorro for a distance of about 20 Km. This horst structure exists near Socorro but not northward in the rift which may suggest an anomalous upper mantle and crustal structure. In support of the crustal anomaly, first olivine tholeiites were identified in the north of New Mexico (Lipman, 1969). This is a magma type that is believed to fractionate at shallow depths (15 to 20 Km). Second are the anomalous heat flow measurements and the numerous hot springs for the Socorro region and the entire rift. A few miles from Socorro a heat flow measurement was made; it was 11.5 HFU, the highest heat flow in the entire state of New Mexico.

Source of Data

The data were divided into two groups. In the first group were the data that had the epicenter location available and in which at least three stations were used for the location calculation. Stations used for the epicenter location calculation were SCC, SNM, SRM, SBB and ALQ. The first four station locations are shown in figure 12. The last station is located 106 Km N24E of SNM. SNM (LRSM), all components, used magnetic tape write out. Magnetic tape write out at a speed of 5 mm/sec was used for correlating phases (figures 4-7) and 25 mm/sec magnetic tape write out was used to time the phases. The second group of data are SNM (NMT) pen and ink helical type of recording with a speed of 4 mm/sec (figure 8). Only the vertical component was recorded. The epicentral distance from SNM station and the depth of focus were calculated from the observed (S-P) and the travel time of S_xS (Sanford, et al., 1973). Depths to the first discontinuity were adopted from Sanford, et al. (1973) for events of located epicenter. For the unknown epicenter location events the depths to the first discontinuity were assumed to be an average value of 18.5 Km.

The characteristics and the response curves of the seismographs used are listed and drawn in Table 2 and figure 1 respectively.

Data, Identification and Analysis

The data selected for this report are gathered in Table 1. Theta in the table represents the angle of emergence from the first layer to the second. The class of the event implies the classification of the

event in relation to the recognizable epicenters with more than one recorded event.

Phase Identification:

A late phase was recognized after the S_XS-phase throughout the seismograms used. It is more defined on the horizontal components of the magnetic tape write out and particularly on the E-W components. The SNM (NMT) records show the later phases with a sharp first arrival. This late phase was named S_ZS. S_ZS is not the result of peculiarity of the station location nor the instramentation because it does show on other stations (figures 9-10). S_ZS cannot possibly be a surface-wave because it does appear on seismograms with energy crossing mountain ranges with elevation many times higher than any reasonable surface-wave wavelength. S_ZS has a sharp impulse on SNM (NMT) records and also it has much higher frequency on the magnetic tape write out than the surface waves arriving later in time.

Data Analysis:

The arrival time of S_ZS and S_XS were plotted as functions of the epicentral distance calculated from the observed (S-P) time interval with P-wave velocity equal to 5.8 Km/sec (Sanford, et al., 1973). Each magnetic tape S_XS phase pick was checked by using it to calculate an epicentral distance and comparing this distance with the one previously used in the epicentral solution. S_XS travel times and the depth to the first discontinuity as given by Sanford, et al. (1973) are used in the following calculations.

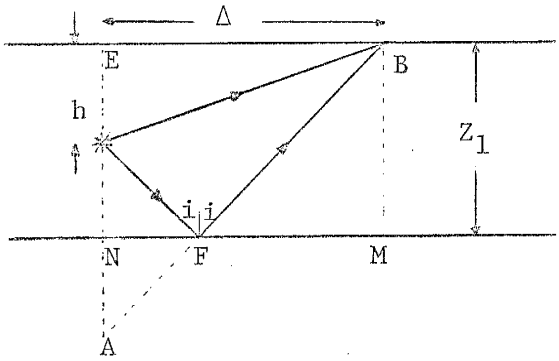

$$(AB)^2 = (EB)^2 + [AN + NC + CE]^2$$

$$(S_xS - O)^2 \cdot V_S^2 = \Delta^2 + (2Z_1 - h)^2$$

$$= [(P - O)^2 \cdot V_P^2 - h^2] + 4Z_1^2 - 4Z_1 \cdot h + h^2$$

$$h = \frac{(P - O)^2 \cdot V_P^2 - (S_xS - O)^2 \cdot V_S^2 + 4Z_1^2}{4Z_1}$$

The epicentral distance = $\Delta = \sqrt{(CB)^2 - (CE)^2}$

$$= \sqrt{(P - O)^2 \cdot V_P^2 - h^2}$$

By comparing the calculated Δ with the measured distance on the map, the epicenter was located using the arcs method. Most of the events fall within ±1 Km difference. The calculated depth of focus h was considered the representative depth of focus of that event and was used later in calculations. The depths of focus were found to range between 6 and 10 Km. The curve representing S_xS fits a theoretical curve of a discontinuity dipping 6° toward the north with a depth immediately under SNM station equal to 17.5 Km. This result checks with the result

reached by Sanford, et al. (1973). Also the arrival times for S_xS and the epicentral distances were corrected for the depth of focus and have been found to match the same theoretical curve the uncorrected data does. The calculations for the depth of focus correction proceeded as follows:

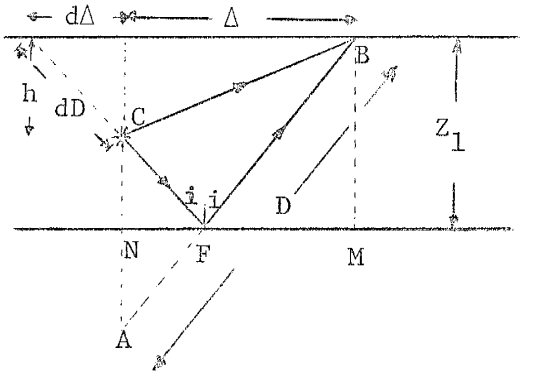

Since $$\frac{Z_1 - h}{Z_1} = \frac{CF}{FB} = \frac{NF}{FM}$$

now first $D = CF + FB$

$$\frac{Z_1 - h}{Z_1} = \frac{CF}{D - CF}$$

$$\therefore \quad CF = \frac{D \cdot (Z_1 - h)}{(2Z_1 - h)} \qquad (1)$$

and similarly

$$NF = \frac{\Delta \cdot (Z_1 - h)}{(2Z_1 - h)} \qquad (2)$$

Also $$\frac{h}{Z_1 - h} = \frac{dD}{CF} = \frac{d\Delta}{NF}$$

From equation (1)

$$\frac{h}{Z_1-h} = \frac{dD\cdot(2Z_1-h)}{D\cdot(Z_1-h)}$$

$$\therefore \qquad dD = \frac{D\cdot h\cdot(Z_1-h)}{(Z_1-h)(2Z_1-h)}$$

$$dt = \frac{(S_xS - O)\cdot V_S\cdot h}{(2Z_1-h)\cdot V_S}$$

$$= (S_xS - O)\cdot\frac{h}{(2Z_1-h)}$$

and from equation (2)

$$\frac{h}{(Z_1-h)} = \frac{d\Delta(2Z_1-h)}{\Delta(Z_1-h)}$$

$$\therefore \qquad d\Delta = \Delta\,\frac{h}{(2Z_1-h)}$$

So by calculating $\frac{h}{(2Z_1-h)}$ which will be named the correction factor the correction for the travel time and the epicentral distance is readily found by multiplying the arrival time or the epicentral distance by the correction factor.

The curves (figure 2) that fit S_xS data points were estimated using a polynomial fit of the second order. The estimated curve had a correlation coefficient equal to 0.99378 and standard error of estimate equal to 0.174.

The S_zS travel times matched curve had a correlation coefficient

equal to 0.995 and a standard error of estimate equal to 0.175 by using only the events that had an epicentral locations.

The $(T^2 - X^2)$ graph (figure 3) gave intercept times to S_xS and S_zS of 8.72 sec and 11.54 sec respectively. Also it gave velocities for the first layer as 3.162 Km/sec for the S-phase and 5.47 Km/sec for P-phase. The measured P-phase velocity is less by 0.33 Km/sec than the velocity given by Sanford, et al. (1973). This may be the result of the dip of the first discontinuity. The graph also gave an average velocity for the first and the second layers of 2.975 Km/sec. The true velocity of the second layer was deduced as follows:

since $$T_1 = \frac{2Z_1 - h}{V_1}$$

$$T_2 = \frac{2Z_1 - h + 2Z_2}{V_a}$$

$$T_2 = \frac{2Z_1 - h}{V_1} + \frac{2Z_2}{V_2}$$

Thus $$V_2 = \frac{(T_2V_a - T_1V_1)}{(T_2 - T_1)}$$

where Z_1 = depth to the first discontinuity

Z_2 = depth to the second discontinuity

V_1 = S-phase velocity in the first layer

V_2 = S-phase velocity in the second layer

V_a = average velocity

Z_2 = thickness of the second layer

T_1 = intercept time of the first layer

T_2 = intercept time of the second layer.

By using the parameters computed from the (T^2-X^2) graph the S-velocity of the second layer was found to be 2.397 Km/sec.

Second Layer Depth Determination:

The depth immediately under Socorro was determined by using the intercept time for the fourth equation on page 7. The depth was found to be 20.88 Km.

The following equations were derived for the calculation of the depth to the second discontinuity:

$$(S_zS-0) = \frac{(2Z_1-h)}{(1-\sin^2 i_1)^{1/2}} \left[\frac{1}{V_1} - \frac{V_1}{V_2^2}\right] + \frac{\Delta \cdot V_1}{V_2^2 \cdot \sin i_1}$$

where i_1, the angle of incidence from the first to the second layer, which is the only unknown, was computed by computer iteration for every travel time (S_zS-0) and the corresponding epicentral distance (Δ). The calculated angle is used for the calculation of the thickness of the second layer in the following equation

$$Z_2 = \left[(S_zS-0) - \frac{(2Z_1-h)}{V_1(1-\sin^2 i_1)^{1/2}}\right] \frac{V_2}{2} \left[1 - (V_2/V_1)^2 \sin^2 i_1\right]^{1/2}$$

$Z_1 + Z_2$ depths are listed in column #8 of Table 1.

Figure 11 shows the depth of the reflecting points on the second discontinuity calculated with the previous formulation. These depths were thus corrected with the knowledge that the depth immediately under SNM station equals 20.88 Km.

Events that originated to the north of SNM station and had a known epicentral location were used to map the second discontinuity (figure 13).

A straight line was fitted to the depth points. The straight line was found to dip 5° to the north from SNM station.

If the assumed second layer S-wave velocity holds for a distance of 40 Km north of Socorro, the depth under that point is found to be 29.69 Km using ALQ seismogram (figure 10).

Characteristics of the Second Discontinuity:

The high frequency and impulsive arrival may suggest that the second discontinuity has a sharp velocity contrast. Also the drop in the amplitude may suggest that a low rigidity material sandwiched between the two discontinuities may be depleting the energy.

Results

The following results may be deduced from the study:

1) A discontinuity having a depth of 20.88 Km is lying immediately beneath Socorro and dipping 5° toward the north.

2) The S-wave velocity of the second layer is 2.397 Km/sec.

3) The low velocity layer may have hot, partially molten material with an increasing thickness north of Socorro. And the whole rift may have patched chambers of hot, low rigidity materials with variable depth that may explain the anomalous heat flow observation to the extent of the Rio Grande rift.

Acknowledgments

The topic of this report was suggested by Dr. Allan R. Sanford to whom I extend my respect for his assistance and guidance throughout this study. Also I would like to express my gratefulness to Esso Libya which made all this possible.

References

Grant, F. S, and West, G. F. (1965). Interpretation Theory in Applied Geophysics, New York, McGraw-Hill Book Company. 584 p.

Richter, C. F. (1958). Elementary Seismology, San Francisco, W. H. Freeman and Company, 768 p.

Sanford, A. R., Alptekin,O., and Toppozada, T. R. (1973), Bull. Seism. Soc. Am. 63, 2021-2034.

Toppozada, T. R. (1974). Seismic Investigation of Crustal Structure and Upper Mantle Velocity in the State of New Mexico and Vicinity, New Mexico, New Mexico Institute of Mining and Technology, Ph.D. dissertation, 155 p.

Table 1

Data Used in the Study

Date	Arrival time at SNM	(S-P)	(S_xS-0)	(S_zS-0)	Δ	h	Depth to 2nd discont.	class of the event	Number on map
12-11-69	19:33:14.6	1.36	8.58	10.76	5.8	9.08	21.86	-	1
7-21-70	08:32:28.1	3.2	11.64	14.27	24.3	7.49	22.83	A	5
10- 2-70	06:19:03.8	3.2	11.8	14.36	24.4	6.94	22.74	A	5
7-21-70	03:54:22.2	3.16	11.63	14.27	24	7.33	22.86	A	5
9-29-70	09:34:24	3.25	11.8	14.38	24.8	7.2	22.76	A	5
11- 9-70	16:09:33.9	3.3	11.78	14.48	25.2	7.6	22.93	A	5
9-27-70	10:36:03.9	2.34	10.3	12.82	17	7.6	22.50	I	4
8-27-69	00:37:02.37	3.3	11.9	14.1	25.2	7.25	22.31	II	3
12- 6-69	22:24:44.1	3.3	11.93	14.09	25.2	7.11	22.26	II	3
9-19-69	00:28:01	1.78	8.78	11.48	10.9	9.1	22.15	V	2
12-28-69	06:15:10.1	2.14	9.65	12.19	15.0	7.8	21.95	V	2
12-28-69	23:38:19.27	2.1	9.58	12.44	14.5	8.38	22.64	V	2
7-23-72	02:36	1.0	8.04	9.62	≃0.0	9.6	20.88	-	-
8-20-72	07:25	1.25	8.23	10.38	2.5	9.6	21.76	-	-
5-31-72	05:47:45.9	1.53	8.87	10.75	8.7	8.6	21.30	-	-
10-28-71	20:02	1.50	8.83	10.73	8.2	8.62	21.44	-	-
11-26-71	14:54	1.58	8.95	10.98	9.2	8.50	21.59	-	-
11- 6-72	18:49:36.2	2.01	9.62	12.07	13.9	7.9	22.10	-	-
10-11-71	03:24	2.16	9.93	12.28	15.4	7.6	22.01	-	-
8- 1-71	05:34	2.31	10.26	13.02	16.9	7.1	22.50	-	-
1-26-72	14:55:43	2.33	10.61	13.09	17.5	6.09	22.12	-	-
1-22-72	10:47	2.46	10.46	13.57	18.3	7.10	22.95	-	-
10-14-71	20:32	2.28	10.3	13.29	17.4	7.3	22.83	-	-
5-13-72	15:50	2.51	10.16	13.32	18.2	8.3	22.08	-	-
5-16-72	22:41:49.2	2.51	10.21	13.09	18.3	8.1	22.78	-	-

Table 2

Characteristics and Period of Operation of Seismographs Used in the Study

(After Sanford, et al., 1973)

Station	System	Type of Recording	Component Recorded Z	NS	EW	Normalized Magnification at 10 HZ	Period of Operation
SNM	NMT	Pen and ink helical, at 4 mm/sec	x			1.3×10^6	7-1-61 to present
SNM	LRSM	Film (Benioff) and magnetic tape.	x	x	x	6.0×10^4	6-8-69 to present
SRM	NMT	Helical film, at 1 mm/sec	x			1.5×10^5	6-25-69 to 6-30-70
SBB	NOAA ASC-1	Magnetic tape with strip chart playback at 4 mm/sec	x	x	x	3.2×10^5	2-15-70 to 12-18-71
SCC	NOAA ASC-1	Magnetic tape with strip chart playback at 4 mm/sec	x	x	x	1.2×10^6	2-26-70 to 11-29-71
ALQ	WWSSN	Film, at 1 mm/sec	x	x	x	2.0×10^4	10-3-61 to present

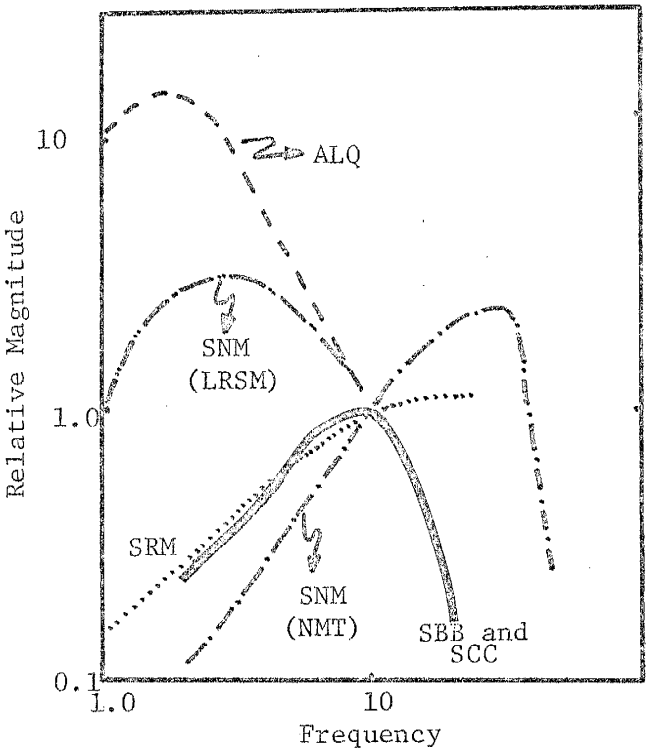

Figure 1

Response curves for all seismographs used in the study. The curve has been normalized to a value of 1.0 at 10 HZ. (After Sanford, et al., 1973).

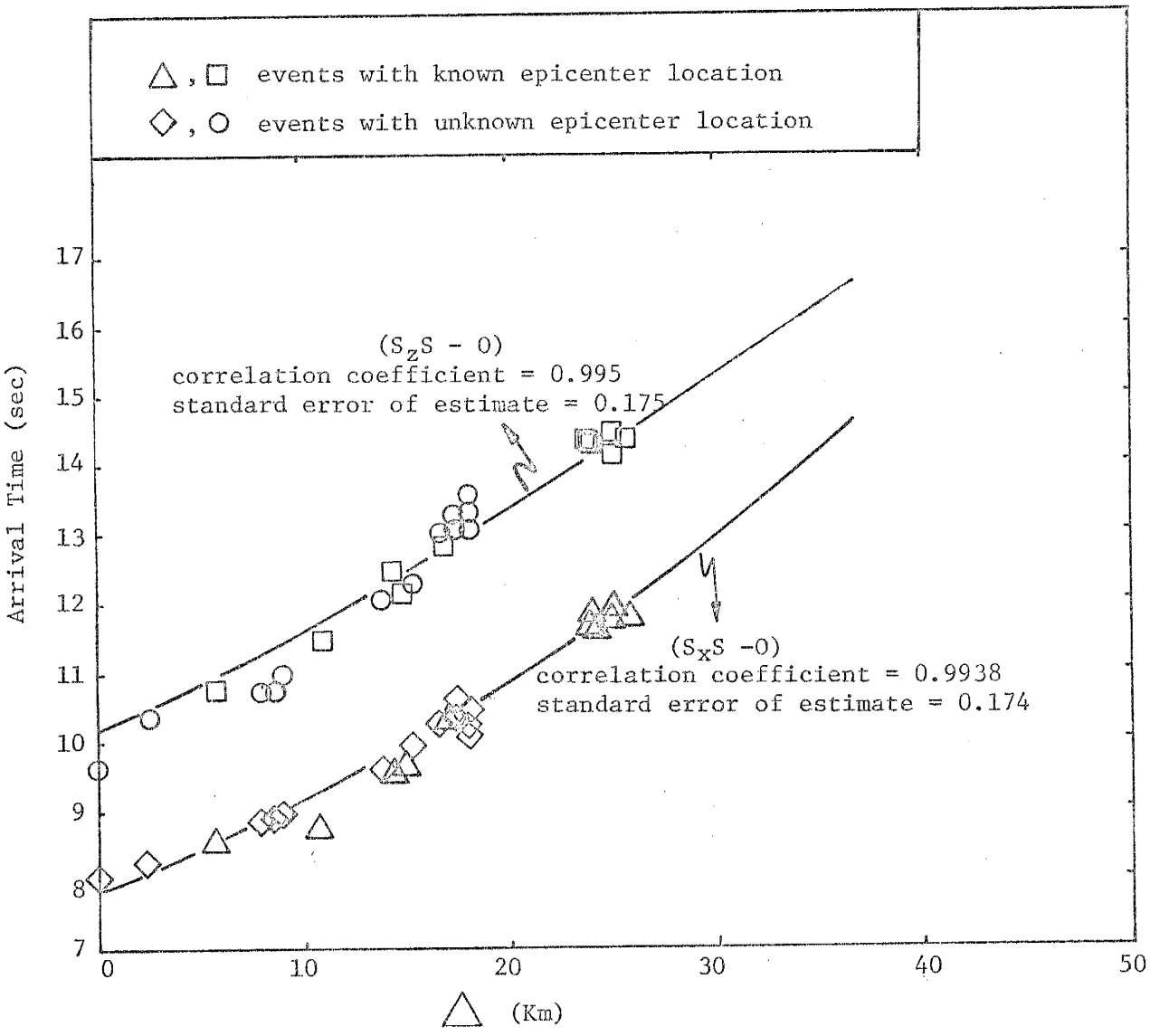

Figure 2

Time-distance curve of the events used.

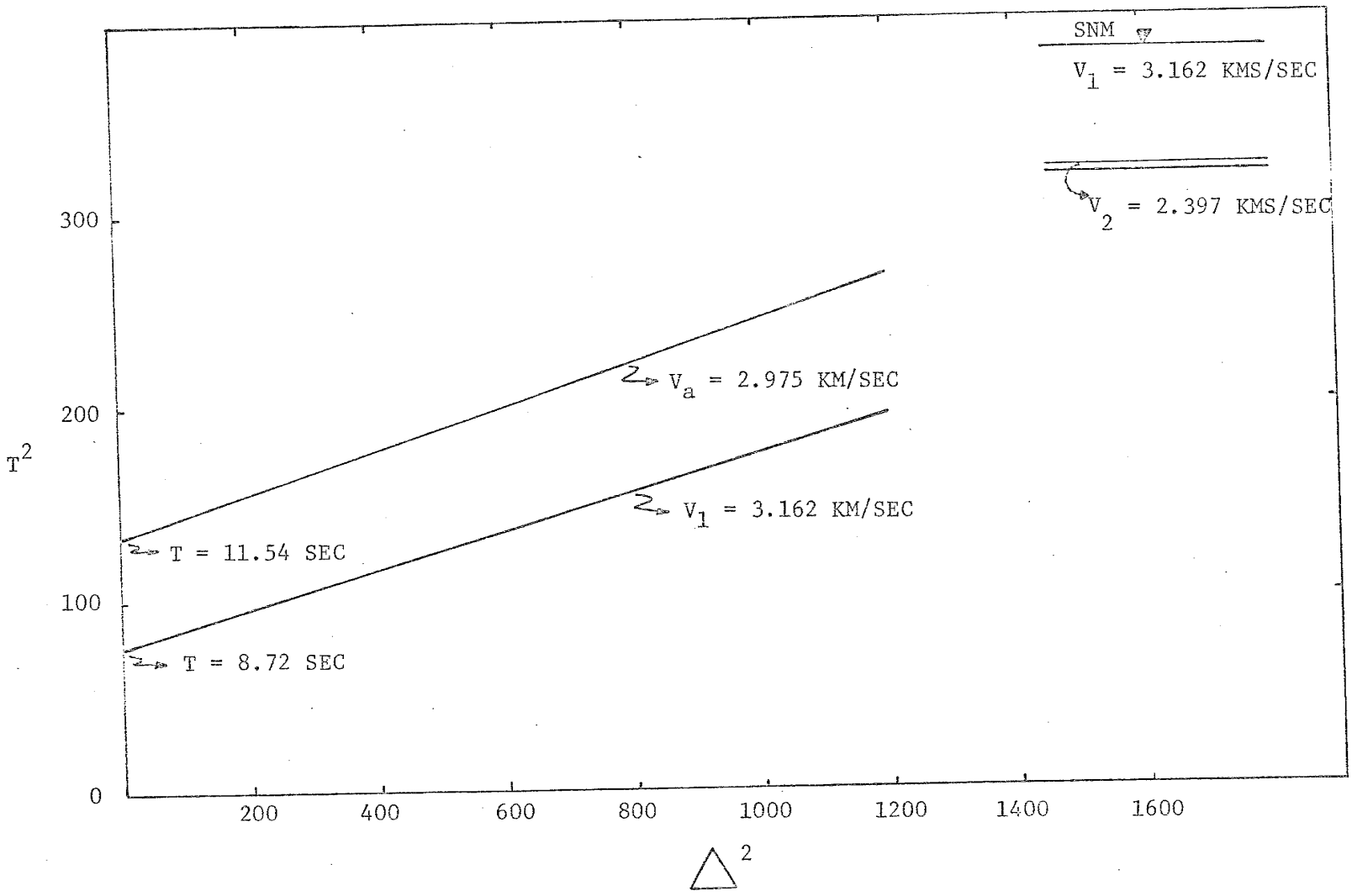

Figure 3

$(T^2 - \Delta^2)$ of the data points.

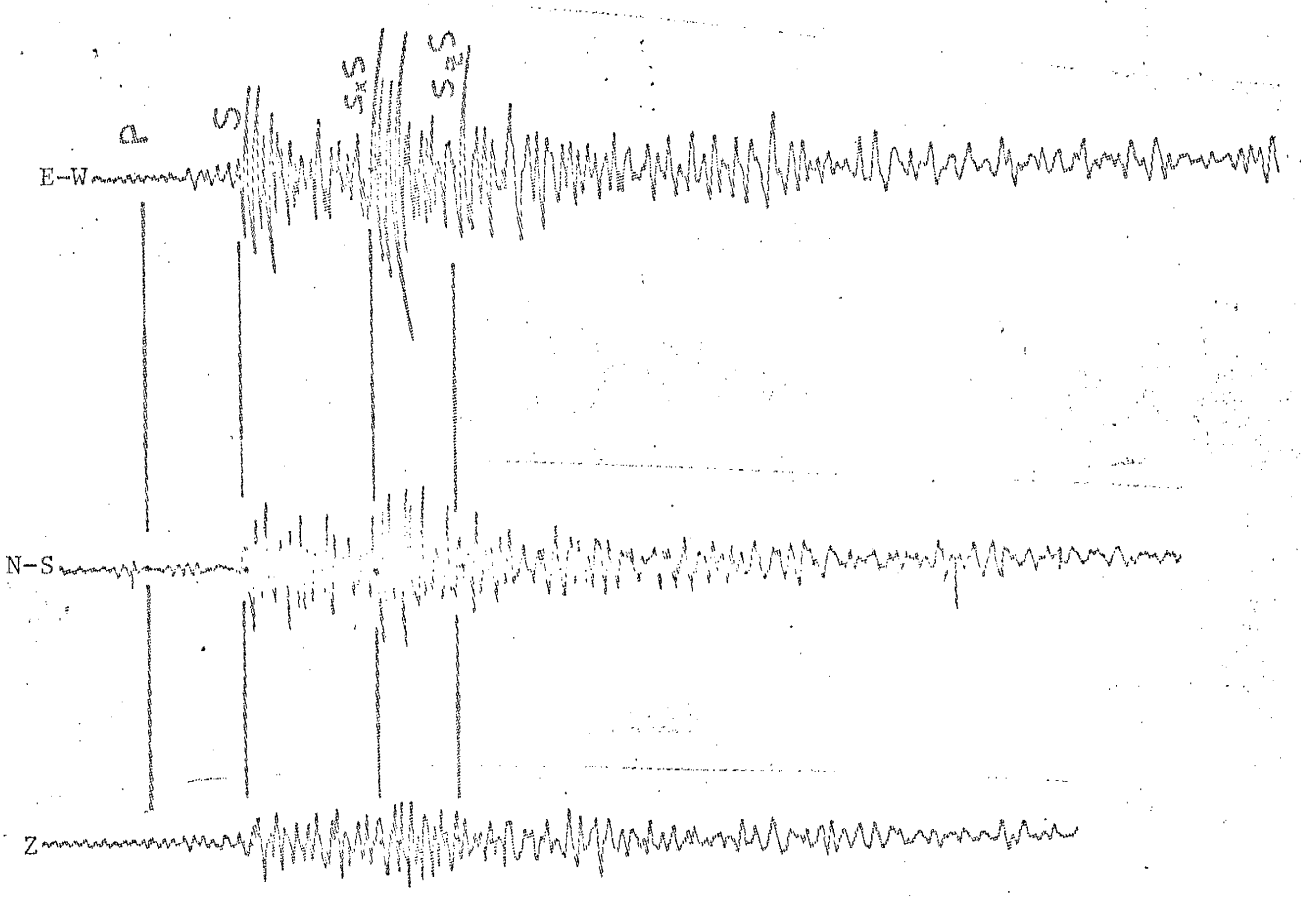

Date: July 21, 1970

SNM Arrival Time: 08:32:28.1

Figure 4

Sample of the microearthquakes used in the second discontinuity study.

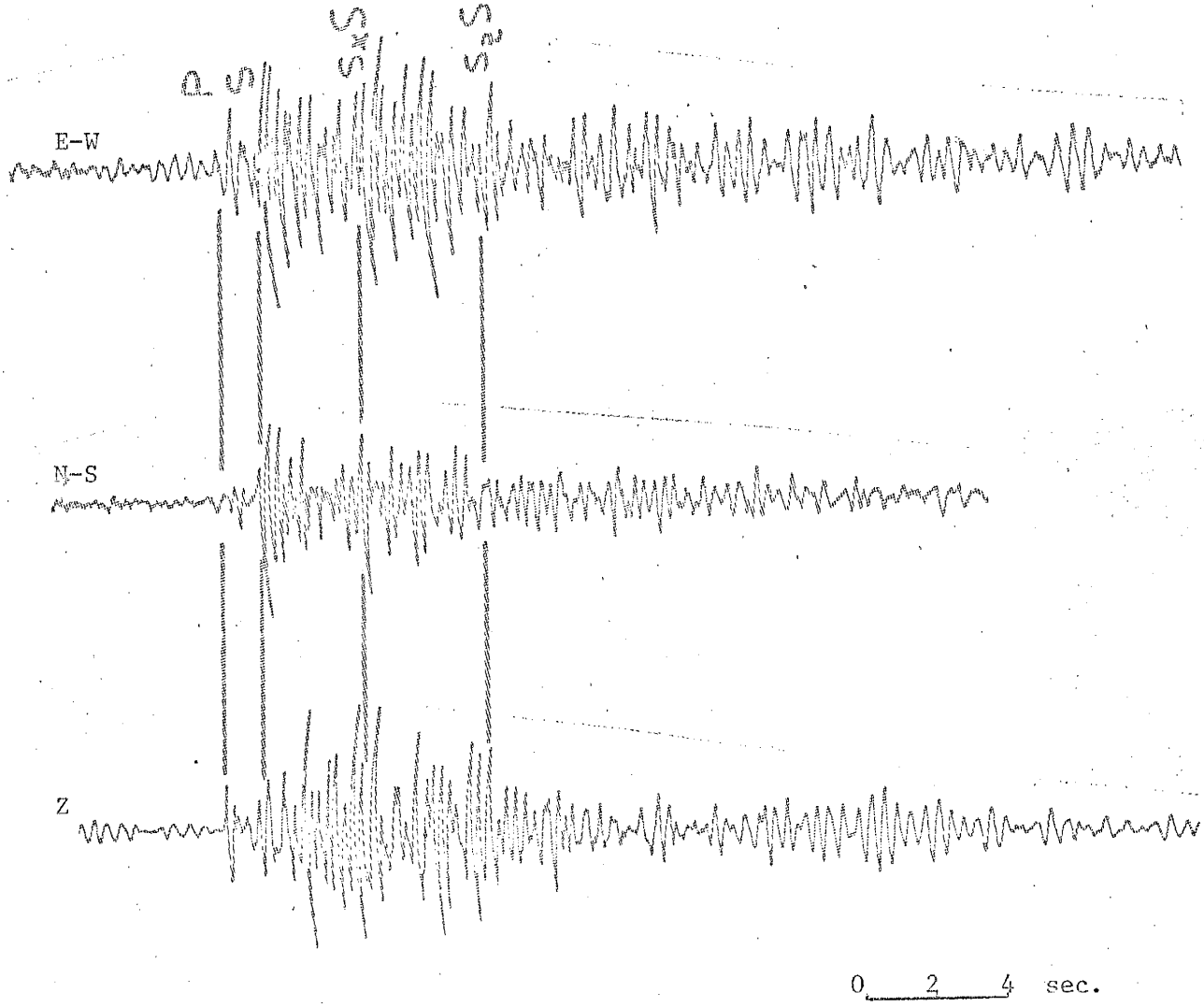

Date: December 11, 1969

SNM Arrival Time: 19:33:14.6

Figure 5

Sample of the microearthquakes used in the second discontinuity study.

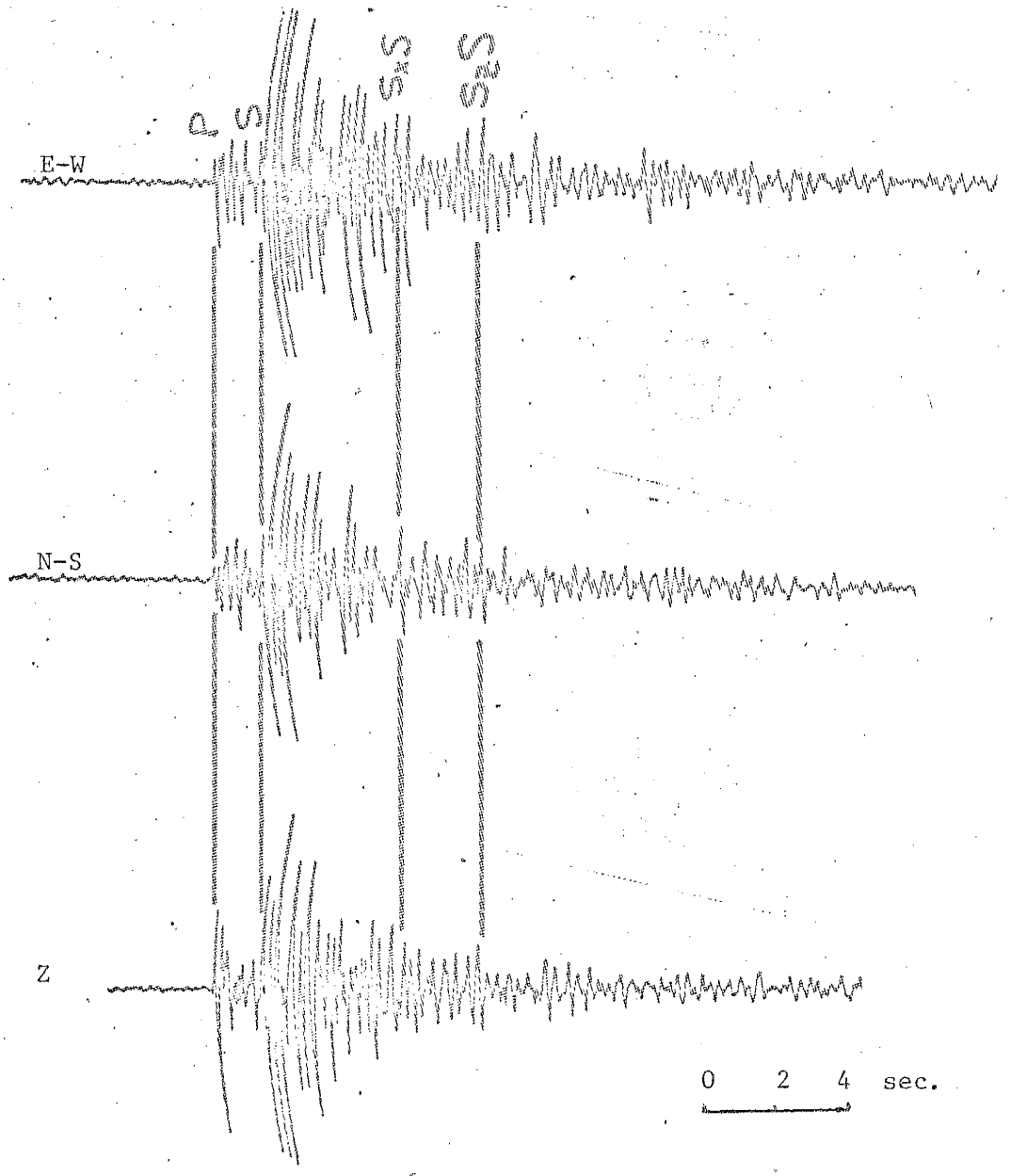

Date: September 19, 1969

SNM Arrival Time: 00:28:01.0

Figure 6

Sample of the microearthquakes used in the second discontinuity study.

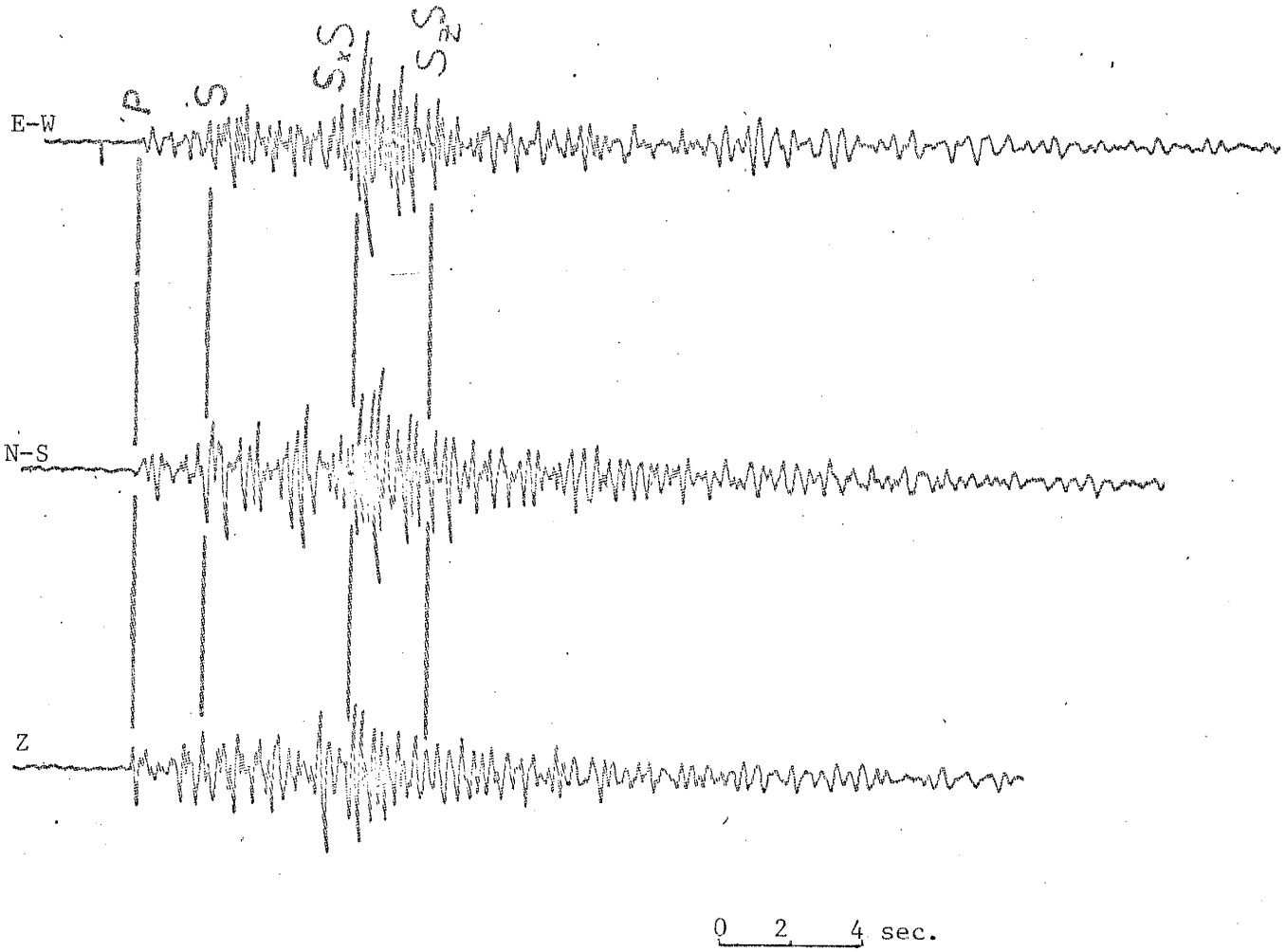

Date: September 27, 1970

SNM Arrival Time: 10:36:03.9

Figure 7

Sample of the microearthquakes used in the second discontinuity study.

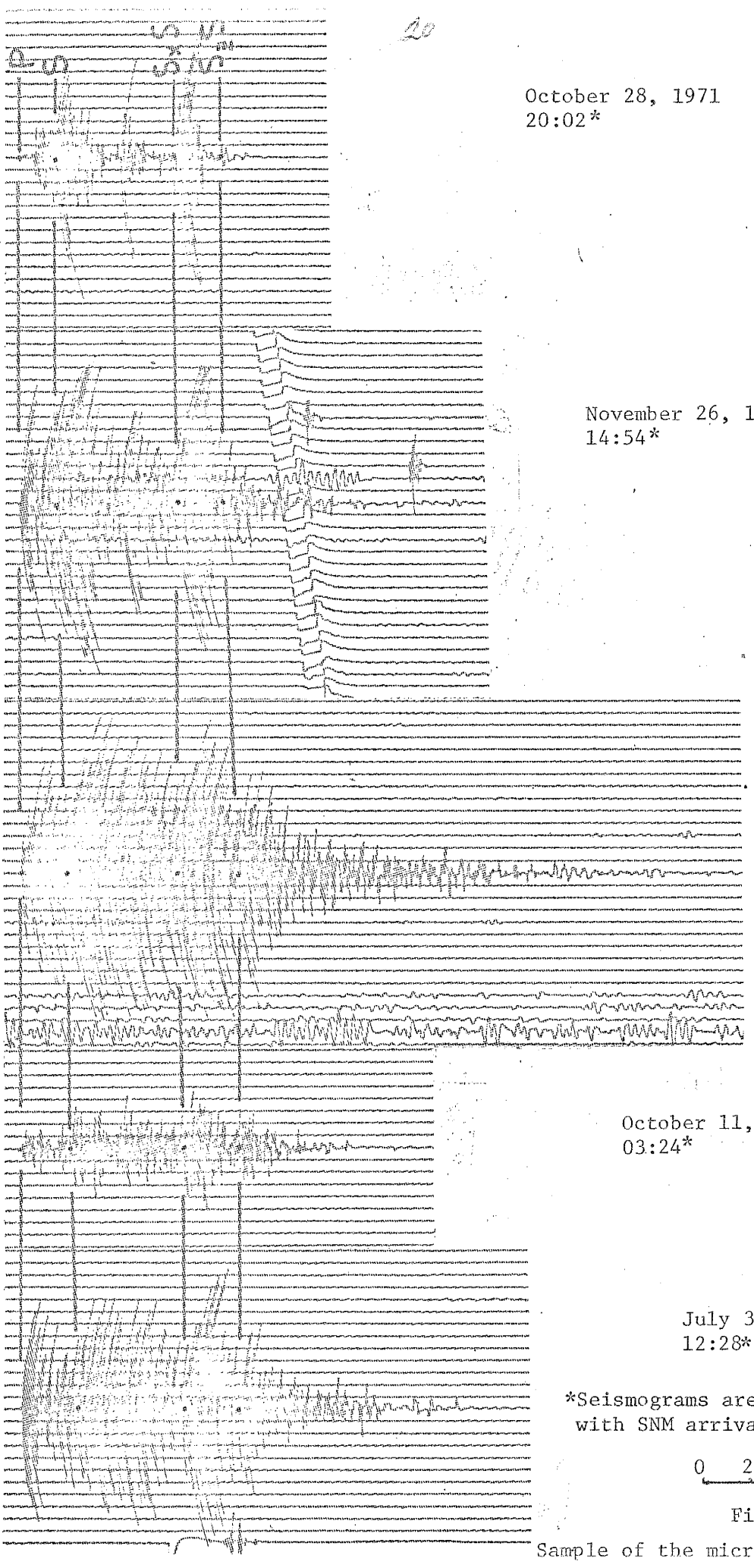

October 28, 1971
20:02*

November 26, 1971
14:54*

November 6, 1972
18:49:36.2*

October 11, 1971
03:24*

July 31, 1972
12:28*

*Seismograms are all Z-component with SNM arrival time.

0 2 4 sec.

Figure 8

Sample of the microearthquakes used.

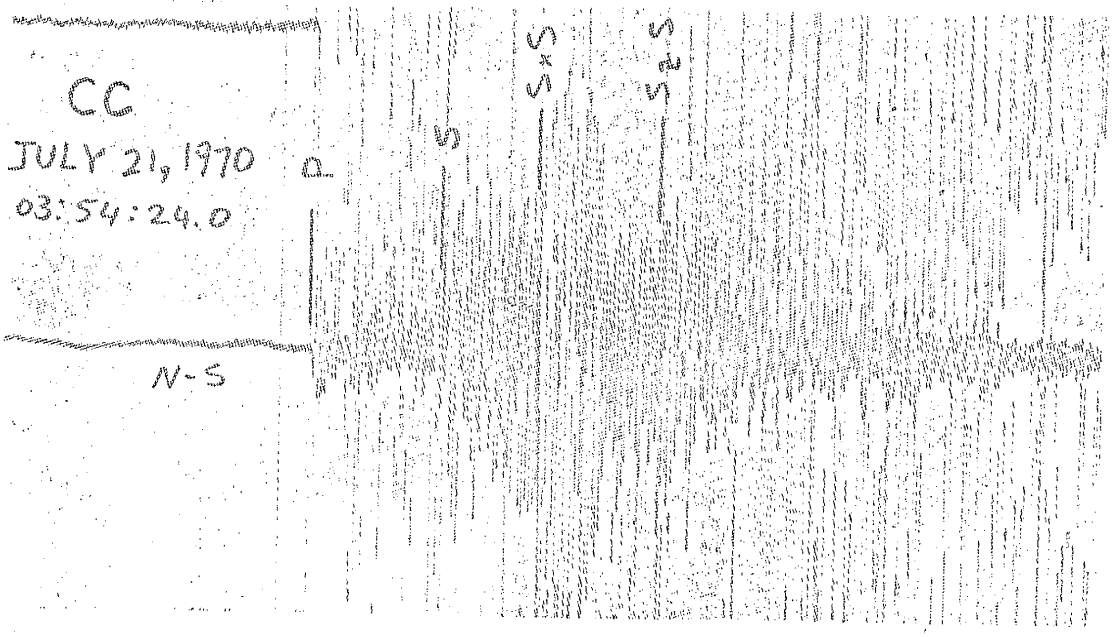

Date: July 21, 1970

SCC Arrival Time: 03:54:24.0

Figure 9

Seismogram from SCC station showing S_zS phase.

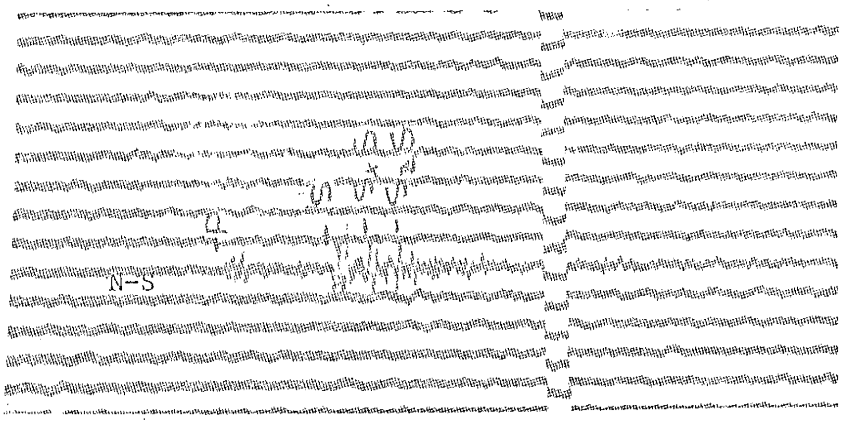

Date: July 21, 1970

Arrival Time at ALQ: 03:54:31.4

Figure 10

Seismogram from ALQ station showing S_ZS phase.

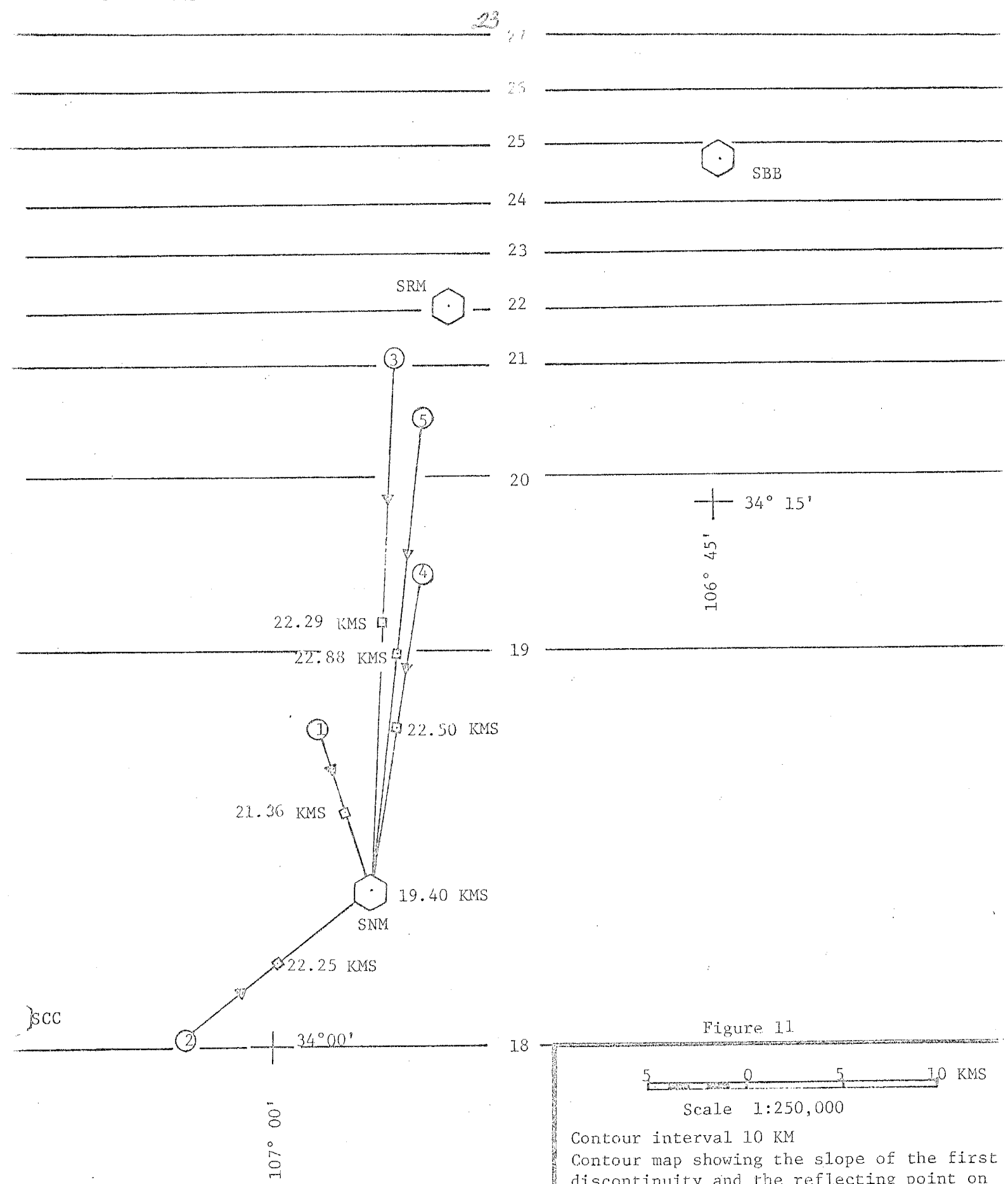

Figure 11

5 0 5 10 KMS

Scale 1:250,000

Contour interval 10 KM

Contour map showing the slope of the first discontinuity and the reflecting point on the second discontinuity with their depths.